The EMBO Journal vol.7 no.12 pp.3829–3836, 1988

Electron microscopic identification of the yeast spliceosome

Michael W.Clark, Susan Goelz[1] and John Abelson

Division of Biology, California Institute of Technology, Pasadena, CA 91125 and [1]Biogen, 14 Cambridge Center, Cambridge, MA 02142, USA

Communicated by E.Brody

We have partially purified the yeast spliceosome by differential sedimentation in glycerol gradients. By electron microscopy we have identified a particle in these fractions that is the spliceosome. In 100 mM KCl buffer, the yeast spliceosome is an ovoid disc with the dimensions of 20 × 23.5 nm with a central indentation. To verify that these ovoid particles were spliceosomes, specific labels were used to tag them. These tagged spliceosomes were then identified in the electron microscope. The salt dependent shift of sedimentation rate for the spliceosome can be explained by a change in size of the particle.

Key words: avidin-biotin/EM/Sm-antibodies/spliceosome/T4 gp32

Introduction

In eukaryotes, mRNA splicing has been found to occur on a large multi-component complex, the spliceosome (Brody and Abelson, 1985; Frendewey and Keller, 1985; Grabowski *et al.*, 1985). This particle can be formed *in vitro* by the addition of exogenous, intron-containing precursor mRNA to cell extracts containing Mg^{2+} and ATP. The spliceosome is composed of a number of proteins and small nuclear RNAs (snRNAs) (for reviews see Sharp, 1987; Maniatis and Reed, 1987). In mammalian pre-mRNA splicing, five essential snRNAs have been identified: U1, U2, U4, U5 and U6. With the exception of U6, these snRNAs possess a trimethyl-guanosine (m^3G) modified nucleotide cap on the 5′ terminus (Mount and Steitz, 1984). The snRNAs are found in particles (snRNPs) containing an snRNA molecule and 6–8 proteins (Mount and Steitz, 1984). The snRNPs are the functional form of the snRNAs in the splicing process. snRNPs U1 and U2 have been shown to have association with the 5′ splice junction and the branch point, respectively (Chabot and Steitz, 1987), of the intron. The yeast snRNAs, snR20, snR19, snR4, snR7 and snR6, although larger, are analogous to mammalian U1, U2, U4, U5 and U6 snRNAs, respectively (Riedel *et al.*, 1987).

Protein factors are also known to be involved in mRNA splicing. The mammalian Sm-antigens are a set of proteins of various mol. wts that share common antigenic determinants and bind to a common sequence, A(U3–6)G, found in snRNAs U1, U2, U4 and U5. In yeast, a set of temperature sensitive mutants, initially isolated by Hartwell (1967), define a set of genes, *rna*2 to *rna*10/11, known to be defective in mRNA splicing at the non-permissive temperature (Rosbash *et al.*, 1981). The protein products of the *RNA* genes have been shown to be directly involved in yeast mRNA splicing process (Lustig *et al.*, 1986). Antibodies directed against the proteins *RNA*8 (Lossky *et al.*, 1987) and *RNA*4 (J.Banroques and J.Abelson, unpublished result), will immunoprecipitate specific snRNAs. In addition, it has been demonstrated that *RNA*11 protein appears to have a direct association with the spliceosome (Chang *et al.*, 1988). In contrast, the *RNA*2 protein appears to act as an extrinsic spliceosome factor (Lin *et al.*, 1987).

Even at this initial level of understanding of the spliceosome constituents, it is obvious that the spliceosome is a dynamic particle of great complexity. The spliceosome assembly process has been analyzed by affinity chromatography (Grabowski *et al.*, 1985) and native PAGE (Konarska and Sharp, 1986; Pikielny *et al.*, 1986; Cheng and Abelson, 1987) for both the mammalian and yeast systems. These experiments have demonstrated that the spliceosome proceeds through several intermediate forms. These intermediates have been shown to contain specific complements of snRNPs.

The orderly assembly of the spliceosome complex implies a specific spatial arrangement of the splicing components. Detailed information on this spatial arrangement for the splicing components requires a high resolution, three-dimensional image of the spliceosome complex. Low resolution images of the *in vivo* mRNA splicing complexes have been obtained by Osheim *et al.* (1985) using the Miller chromatin spreading techniques. Viewing spreads of nascent transcripts of the *Drosophila* chorion s36-1 and s38-1 genes by EM, they observed particles on these transcripts that the data suggested were RNPs. A 40-nm diameter particle was found that appeared to represent the coalescence of two smaller 25-nm diameter particles. The position of these smaller particles on the transcripts corresponded well with the positions of the 5′ and 3′ splice junctions for the intron in the nascent transcripts. The larger 40-nm particle, presumably the spliceosome, appears to maintain the proximity of the splice site junctions during the intermediate stages of mRNA splicing. More recent work from Beyer and Osheim (1988) demonstrated that the 3′ splice junction RNP particle appears first, followed by the 5′ site particle. This sequence of splice junction recognition correlates with the order of splice site selection known from biochemical assays (Bindereif and Green, 1987).

The nascent transcript spreading technique yields low resolution images of the spatial ordering of major mRNA splicing events *in vivo*, the metal-shadowing required for this method, however, obscures any structural information about the individual spliceosome complexes. To reveal such structural information about the spliceosome requires reasonably pure preparations of this complex. We have produced such a preparation of spliceosomes by forming the complexes *in vitro* from yeast extracts, and then purifying them by differential glycerol gradient sedimentation at different salt concentrations. We have examined peak fractions from these gradients by EM and thereby visualized the yeast spliceosome. We present evidence to substantiate the identity of this image as the spliceosome complex. Oligomerized streptavidin, T4 gp32, and IgG against spliceosome proteins, were used to tag specific spliceosome constituents. These tagged complexes were isolated and then visualized in the electron microscope. We also describe a change in dimensions of the spliceosome as a result of the KCl concentration.

Results

Examination of the 40S spliceosome fraction

In yeast, mRNA splicing components are only a minor fraction of the cell constituents. This fact has hindered us from obtaining preparative quantities of intact spliceosome complexes. Nevertheless, small, partially purified quantities of spliceosomes have been isolated by taking advantage of a change in sedimentation of the spliceosome caused by variation in the monovalent cation concentration (Brody and Abelson, 1985). Increased KCl concentration in a glycerol gradient causes a retarded migration of the spliceosome in the gradient. We believe that this change in sedimentation is not due to major loss of components. Spliceosomes, when centrifuged in one salt concentration, then rerun in a different salt concentration, will run at the appropriate sedimentation rate for that salt (data not shown). We have used this 'salt shift' characteristic to purify the spliceosome for electron microscopic identification.

When the concentration of KCl in the glycerol gradient is 400 mM, the spliceosomes sediment slowly at ~25S (Figure 1A). When the salt concentration is decreased to 50 or 25 mM, the spliceosomes sediment much faster, 40S and greater. When the KCl concentration is 100 mM they sediment at 34S in the glycerol gradient (Figure 1B). (In the remainder of the paper this 34S peak will be referred to as the 40S peak.) This 'salt shift' is not seen with other cellular components in the pre-mRNA splicing extract, namely: 40S ribosomal subunits, fatty acid synthetase, sedimenting at about 29S (see arrows in Figure 1A and B indicating the positions of these particles in the gradients) or lipid vesicles. When the splicing mixture was centrifuged, first on a gradient containing 400 mM KCl (Figure 1C), most of the faster sedimenting particles (40S ribosomes) were removed from the spliceosome-containing fractions. Centrifugation of these fractions on a subsequent gradient containing 25 or 100 mM KCl (Figure 1D) removed most of the slower sedimenting particles (fatty acid synthetase). An advantage of this sequence in the 'salt shift' purification scheme was that after the 400 mM salt gradient (Figure 1C) the spliceosomes were in fractions which contain relatively low amounts of glycerol (11%). These spliceosome fractions could thus be layered directly on the low salt gradient (Figure 1D) which contains higher concentrations of glycerol (15–27%). Spliceosomes which had been purified on sequential glycerol gradients were stained for EM by the single-layer carbon staining technique for visualizing macromolecules (Lake, 1979). In this way, a particle which is most likely the yeast spliceosome was identified.

Figure 2 shows a gallery of the spliceosome particles seen in fractions from a final gradient containing 100 mM KCl. The particle was a disc-shaped ovoid with a central indentation. This particle had the dimensions of 20 × 23.5 ± 1.5 nm. These particles made up ~32% of the particles observed (see Table I). The majority of the images seen in the 40S peak fractions were of the 40S ribosomal subunit (~64%, see Table I). A minor portion of the particles seen resembled the fatty acid synthetase complex (~5%, see Table I). Both of those latter particles were easily identifiable by their distinctive structure and size (Stoops *et al.*, 1978; Lake *et al.*, 1984). Control experiments were done by leaving the ATP out of the mRNA splicing mixture. ATP is required for mRNA splicing and for formation of the 40S

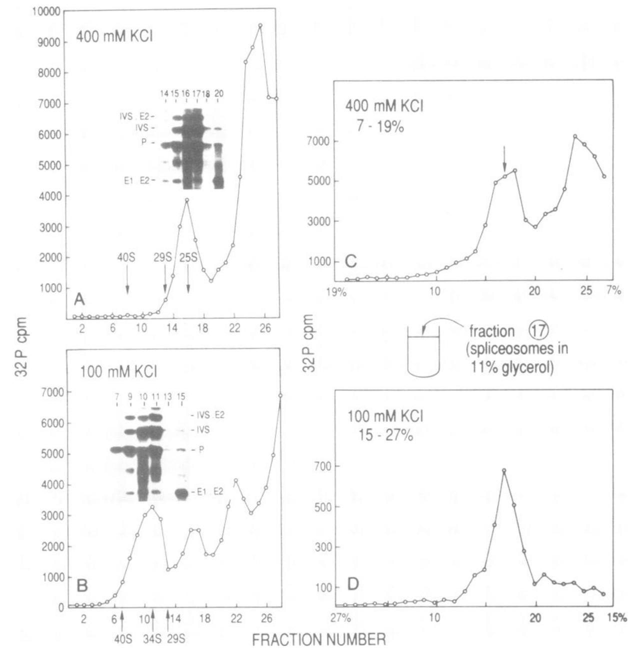

Fig. 1. Glycerol gradient profiles of the yeast spliceosome. (A) and (B) show the effects of different KCl concentrations on the sedimentation rate of the yeast spliceosome. (**A**) The sedimentation profile of a yeast mRNA splicing reaction centrifuged through an 11 ml, 15–27% linear glycerol gradient made in a buffer containing 400 mM KCl. The spliceosome peak sediments at ~25S relative to the yeast 40S ribosomal subunit (see the arrow labeled 40S). The insert above the 25S peak is the autoradiograph of aliquots of the indicated fractions that have been electrophoresed on a denaturing polyacrylamide gel. The resulting bands reveal that all of the expected mRNA splicing intermediates are contained within this peak. (**B**) The sedimentation profile of an mRNA splicing reaction centrifuged through a similar 11-ml gradient as in (A) except the KCl concentration was 100 mM. In this gradient the spliceosome sediments at 34S relative to the 40S ribosomal subunits (see arrows labeled 40S). The insert above the 34S peak shows that all of the expected mRNA splicing intermediates are contained in this peak. The arrow labeled 40S indicated where the yeast 40S ribosomal subunit sediments in the perspective gradient. The arrow labeled 29S indicated where the yeast fatty acid synthetase sediments. Fraction 26 is the top of the gradient. IVS.E2, intron and exon 2; IVS, intron lariat; P, pre-mRNA; E1.E2, mature mRNA. (C) and (D) are the gradient profiles of the double gradient purification scheme used to isolate the yeast spliceosome for EM identification. (**C**) The profile of a yeast mRNA splicing reaction layered on an 11 ml, 7–19% linear glycerol gradient containing 400 mM KCl and centrifuged as indicated in Materials and methods. The spliceosome peak fraction, number 17 (the large arrow), now in ~11% glycerol, was then loaded onto a 5 ml, 15–27% linear glycerol gradient containing 100 mM KCl and centrifuged as indicated in Materials and methods. (**D**) The profile of this 100-mM KCl gradient.

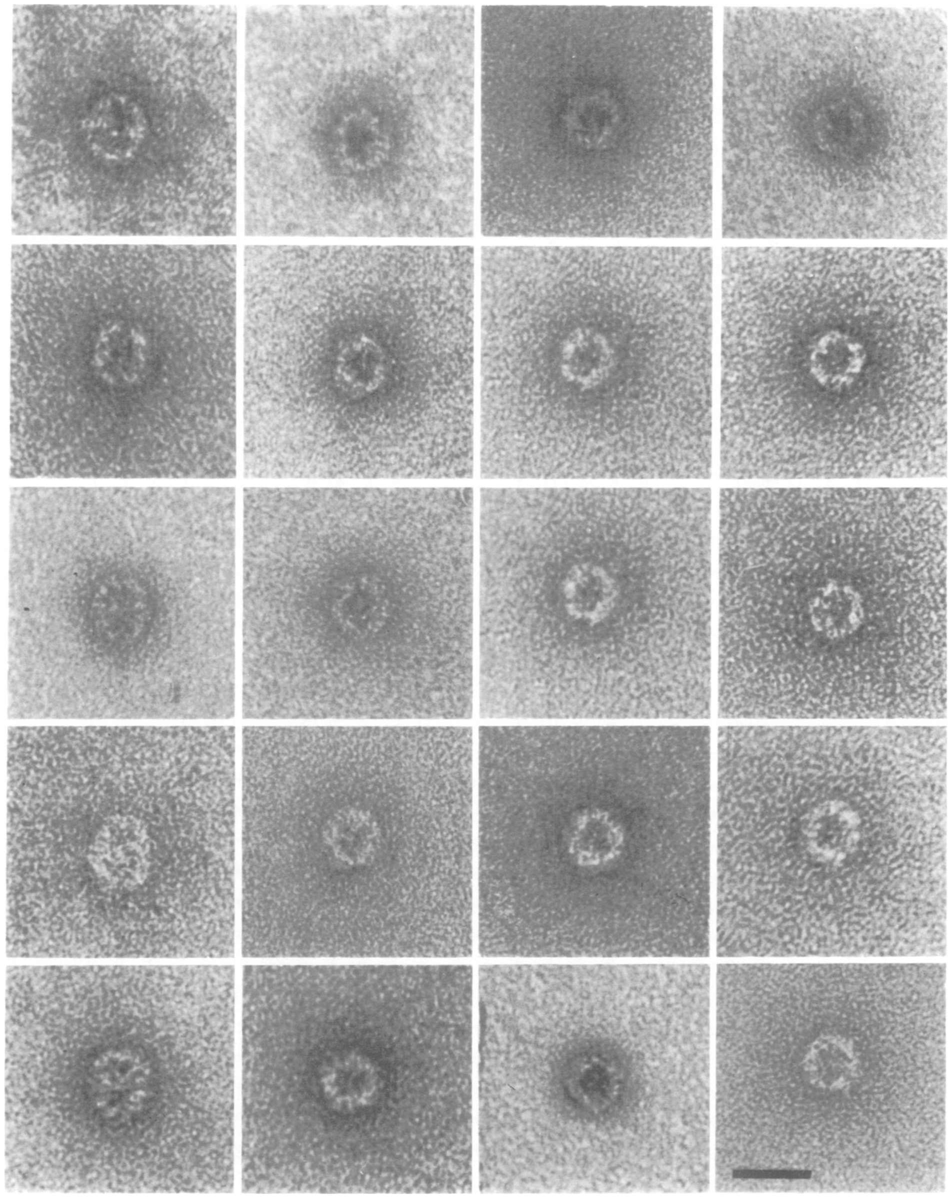

Fig. 2. A gallery of electron microscopic images of the spliceosome particle purified by the double glycerol gradient purification procedure. Immediately upon fractionation of the final 100-mM KCl containing gradient, glutaraldehyde was added to each fraction to make a concentration of 0.3%. The radioactivity profile was determined and the 40S peak fractions were stained for EM by the single-layer carbon method (Lake, 1979). The average size of the ovoid particle on the left side of the gallery was $20 \times 23.5 \pm 1.5$ nm. The average size of the more circular particle on the right side of the gallery was $20 \times 20 \pm 1.5$ nm. Bar = 25 nm.

complex. In the absence of ATP a 30S complex forms instead. For the control experiments, fractions were taken for the EM staining, from the region of the gradient that corresponded to the 40S peak. These fractions showed only 40S ribosomal subunits and some fatty acid synthetase (data not shown). Other control experiments were performed. One of these used labeled RNA transcripts containing no pre-mRNA splicing signals (Brody and Abelson, 1985) (the antisense of the actin pre-mRNA), which formed a 25S sedimenting peak. Another experiment was done in the absence of pre-mRNA transcript. Similar results were obtained for both experiments. That is, the 40S ribosomes, fatty acid synthetase complex and other unidentified particles were seen, while the ovoid particles were absent. The appearance of these ovoid particles in the region of 40S sedimentation was dependent upon the presence of exogenous pre-mRNA that contained the proper splicing specific signal sequences and the presence of ATP. These conditions are also required for the formation of the 40S spliceosome peak in the gradient. From these results the ovoid particle is most

Table I. Particles in leading and peak fractions of a 100 mM KCl spliceosome gradient

Fraction no.	Total particles	Spliceosomes	40S Ribosomes	FAS[a]
16	62	18 (29%)[b]	40 (64.5%)	4 (6.5%)
17	138	44 (32%)	89 (64.5%)	5 (3.5%)
18	306	110 (36%)	193 (63.0%)	3 (1.0%)

[a]Fatty acid synthetase.
[b]The numbers in parentheses are percentages of all particles counted.

Table II. Spliceosome and 40S ribosome density in leading and peak fractions of a 100-mM KCl spliceosome gradient

Fractions	^{32}P c.p.m.	Spliceosomes per square micron	40S ribosomes per square micron
16	460	0.0120	0.0301
17	780	0.0310	0.0627
18	1060	0.0471	0.0822
Fraction ratios	c.p.m.	Spliceosomes	40S ribosomes
17/16	1.69	2.58	2.08
18/17	1.36	1.52	1.31

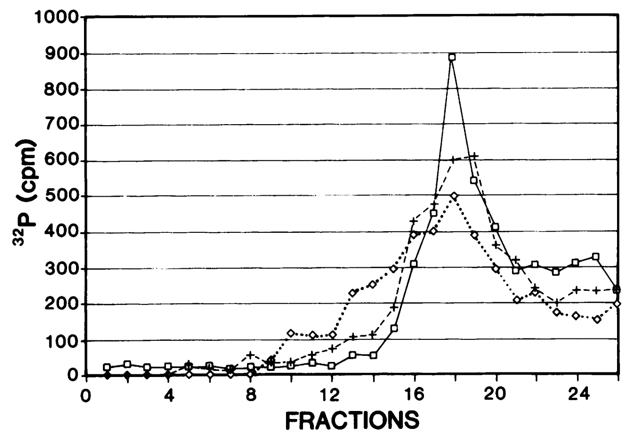

Fig. 3. The addition of oligostreptavidin (OSA) rods to the spliceosome formed on biotinylated pre-mRNA caused the increase in sedimentation of these particles. OSA rods were added to the sample after the first 400-mM KCl gradient, incubated with the spliceosome fractions for 15 min at 8−10°C and then centrifuged on a 100-mM KCl gradient. Crosses, spliceosomes formed on 2% biotinylated-uridine containing pre-mRNA plus 0.1 pg of OSA rods. Diamonds, spliceosomes formed on 2% biotinylated-uridine containing pre-mRNA plus 1.0 pg of OSA rods. Squares, spliceosomes formed on pre-mRNA containing no biotinylated nucleotides plus 1.0 pg of OSA rods.

likely the spliceosome. Further evidence for this conclusion was obtained by determining the density of these ovoid particles relative to the amount of ^{32}P radioactivity in the 40S peak fractions.

Because of the low amount of spliceosomes formed in an mRNA splicing reaction, ~0.1 fmol, a high concentration of these spliceosome particles could not be produced. Consequently, high magnification electron micrographs containing many spliceosome particles could not be obtained. Still, a correlation between ^{32}P radioactivity in the 40S fractions with the density of spliceosome particles seen in the electron microscope was found. Simply by counting the number of spliceosomes that appeared in a calculated area in low magnification electron micrographs, densities for the spliceosomes and the 40S ribosomes were determined for each fraction (Table II). The leading and peak fractions of the 100-mM KCl gradient (see Figure 3, squares, fractions 16−18) were examined for this purpose. In each fraction, 16−18, correspondence was revealed between the radioactivity in a fraction and the density of the ovoid particles on the grid (Table II). The ratios for fractions 18 and 17 were almost the same. The ratio of 40S ribosome densities showed the same trend, but the 40S ribosome and the spliceosome have approximately the same sedimentation rate at 100 mM KCl and should demonstrate similar behavior.

There was an observable heterogeneity in these ovoid particles. A majority of the particles (88%) were more ovoid, 20 × 23.5 ± 1.5 nm in dimensions (see Figure 2, the leftmost images), while a minority of the images (12%) were more circular, 20 × 20 ± 1.5 nm in size, (Figure 2, the rightmost images). This heterogeneity could be the result of the fixation of these particles with 0.3% glutaraldehyde (Valentine *et al.*, 1968), which was necessary for particle survival during the staining process, or it could represent the various spliceosome intermediates identified on native gels that are contained within the 40S spliceosome peak fraction (Konarska and Sharp, 1986; Pikielny *et al.*, 1986; Cheng and Abelson, 1987). The spliceosome specific labeling experiments described below, however, contain these different sizes and shapes for the spliceosome particles observed here. These data indicate that all of these images are representative of the 40S spliceosome particle.

Oligostreptavidin rods bind to spliceosomes formed on biotinylated intron-containing precursor mRNA

Further evidence that the image reported here is the spliceosome comes from electron microscopic techniques used specifically to label macromolecules (Lake *et al.*, 1984; Oakes *et al.*, 1986). In the first labeling experiment, biotinylated-uridine was incorporated into the pre-mRNA. This biotinyl-pre-mRNA still formed yeast spliceosomes (Figure 3, crosses and diamonds, fraction 18 is the 40S peak fraction) and could be efficiently spliced (data not shown). Biotinylated-uridine-containing pre-mRNA has also been shown to form spliceosomes in mammalian systems (Grabowski *et al.*, 1986). The sedimentation rate of the spliceosome formed with the biotinyl-pre-mRNA could be increased by adding increasing amounts of oligomerized streptavidin (OSA) (Figure 3, crosses, 0.1 pg OSA, diamonds, 1.0 pg OSA). The addition of OSA to spliceosomes formed on unbiotinylated pre-mRNA, as a control, showed no increase in sedimentation rate (Figure 3, squares, 1.0 pg OSA). Electron microscopic examination of all the major fractions of these gradients revealed that the increase in sedimentation was caused by polymerization of the biotinyl-spliceosomes through the multiple binding sites of the OSA (data not shown). Because too much polymerization of the spliceosomes obscured the visualization of the complexes, the images shown here for this labeling experiment come from a gradient with a low concentration of OSA added (0.1 pg, the leading shoulder fraction 16 from Figure 3, crosses). Figure 4, rows A and C show examples of what was observed. In this experiment 40% of the spliceosomes were labeled with the OSA (the percentages are corrected for any background aggregation or OSA attachment seen in a parallel labeling experiment done with unbiotinylated pre-mRNA) (Figure 3, squares). Figure 4B depicts images of the negatively stained OSA rods used for the labeling experiment. The OSA rods consist of 4−6 streptavidin molecules linked by a bifunctional biotin reagent (Green *et al.*, 1971). Forty-seven per cent of the particles observed were individual spliceosomes with OSA rods attached (Figure 4, row A). Figure 4, row C, shows the biotinyl-spliceosome particles dimerized by OSA rods. Dimers of spliceosomes represent 34% of the OSA labeled particles. The remaining labeled biotinyl-spliceosomes were larger aggregates of particles. These particles, taken from a

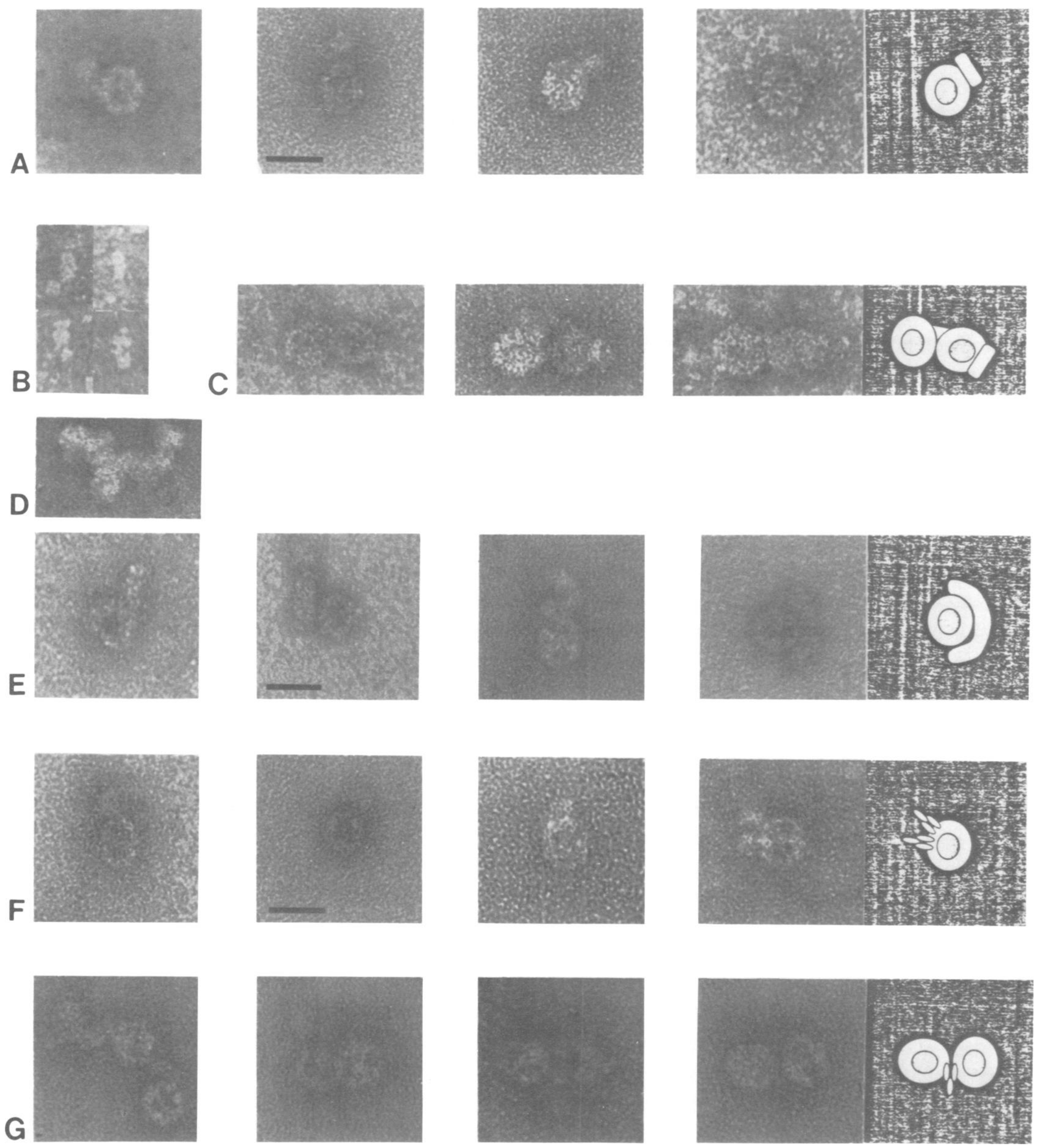

Fig. 4. A gallery of spliceosomes labeled for spliceosome components. These particles were first taken from a 400-mM KCl containing glycerol gradient, the spliceosome specific label was added, the samples were incubated at 8−10°C for 15 min and then the samples were layered on a second gradient containing 100 mM KCl. Rows **A** and **C** are images of particles formed on 2% biotinylated-uridine containing pre-mRNA plus 0.1 pg of OSA rods. **B** is four images of the OSA rods used to stain the biotinylated spliceosomes seen in rows A and C. A, single spliceosome particles with a single OSA rod attached (see diagram at the end of the row), C, images of two spliceosome particles linked by the OSA rods (see the diagram at the end of the row). ***D*** is the thick, filamentous fiber formed when 6 ng of T4 gp32 has been added to 0.1 fmol of pre-mRNA. Row **E**, spliceosome particles which have had 6 ng of T4 gp32 added to 0.1 fmol of spliceosomes. The filaments attached to the spliceosomes vary in length from 20 nm (left) to 60 nm (right) accounting for 10−30% of the possible length of the pre-mRNA which was composed of 605 nt. Rows **F** and **G** are spliceosomes taken from a gradient to which 15 ng of anti-Sm58 IgG were added. Row F, individual spliceosomes with IgG attached. The diagram at the end of the row shows two sites of IgG binding. Row G, multiple spliceosomes linked by anti-Sm58 IgG. The first image in the row is a trimer, while the rest are dimers linked by the anti-Sm58 IgG (see the diagram at the end of the row). Bar = 25 nm.

100-mM KCl gradient, have the same appearance as those seen in Figure 2 under the same salt conditions. Furthermore, the first two dimerized spliceosomes in Figure 4, row C, show ovoid and circular particles attached by OSA rods. This crosslinking of the two types of particles demonstrates that these two images are both spliceosomes.

T4 gene 32 product binds to the spliceosome particles

Another pre-mRNA marker was used for the T4 gene 32 product. It was found that the protein product of bacteriophage T4 gene 32, which binds to ss DNA and RNA (Newport *et al.*, 1981), would bind to spliceosomes. Presumably, the T4 gp32 was binding to pre-mRNA not completely bound up in the spliceosome complex. To get sufficient binding of T4 gp32 to the particle, the spliceosome fraction from a 400 mM KCl-containing gradient had to be diluted with buffer to make the KCl concentration 100 mM. When these samples were subsequently centrifuged on a 100-mM KCl-containing glycerol gradient the 40S peak had a distinct shoulder on its leading edge (similar to the shoulder seen in the OSA gradient in Figure 3, diamonds). Fractions from this shoulder examined by EM revealed spliceosome complexes that had thick filamentous protrusion of variable length attached (20–60 nm) (Figure 4, row E). T4 gp32 and pre-mRNA alone under the same buffer conditions showed only thick filaments of a similar structure (Figure 4D). In this case, though, the filaments were longer, ~110 nm in length, which is 55% of the predicted length of a polynucleotide composed of 605 bases. The pre-mRNA and T4 gp32 filaments also appeared slightly more aggregated (Figure 4D) than the shorter filaments seen attached to the spliceosomes (Figure 4, row E). The increase in sedimentation of the spliceosomes appeared to be caused by the increase in length of these filaments. This increase in filament length was presumably the result of attachment of more T4 gp32 protein to the pre-mRNA.

Antibodies to spliceosome components bind to the spliceosome particle

Another labeling experiment was done which targeted the spliceosome proteins. Two antibodies directed against yeast spliceosome proteins were used as markers. One antibody was a human autoimmune serum Sm58 which will immunoprecipitate yeast spliceosomes (Chang *et al.*, 1988). Riedel and co-workers (1987) and Tollervey and Mattaj (1987) have reported that a few of the anti-Sm sera will also precipitate yeast snRNPs. When an Sm58 IgG fraction was incubated with 40S spliceosome fractions containing 400 mM KCl and subsequently centrifuged on a 100-mM KCl gradient, a leading shoulder formed on the 40S peak. The shape of the spliceosome peak was similar to that seen in Figure 3, crosses. Electron microscopic examination of these leading shoulder fractions (equivalent to Figure 3, crosses, fractions 16 and 17), revealed spliceosomes that had IgG molecules attached (Figure 4, rows F and G). In this experiment 35% of the spliceosomes showed attachment of one or more IgG molecules. (The percentage background labeling seen in a non-immune IgG experiment has been subtracted from the labeling figures for the immune experiments). Sixty per cent of the labeled particles in the anti-Sm58 experiment occurred as monomers (Figure 4F), while 22.5% were dimerized by the Sm58 antibody (Figure 4, row G, the rightmost images). The remaining labeled spliceosomes occurred as trimers (Figure 4, row G, the left most image). Furthermore, an antibody raised against a yeast spliceosome component *RNA*11 (Chang *et al.*, 1988) was used to tag the spliceosome particle for EM. This antibody bound to the same particle as the anti-Sm58 antibody (data not shown) but with slightly less binding affinity. Only ~18% of the spliceosomes were labeled with the anti-*RNA*11 antibody over preimmune antibody background staining. For both of these antibodies, the labeled particles were the same size and shape as the particles described above that were deemed to be the spliceosome.

The changes in monovalent cation concentration change the dimensions of the spliceosome particle

To determine if there was some structural explanation for the salt-dependent sedimentation rates of the spliceosome, fractions from spliceosome gradients containing different salt concentrations were examined (Figure 5). The difference in salt concentrations affected the overall size of the particle: at 25 mM KCl (Figure 5, row A) the spliceosome dimensions were 16 nm × 18 ± 1.5 nm, at 100 mM KCl

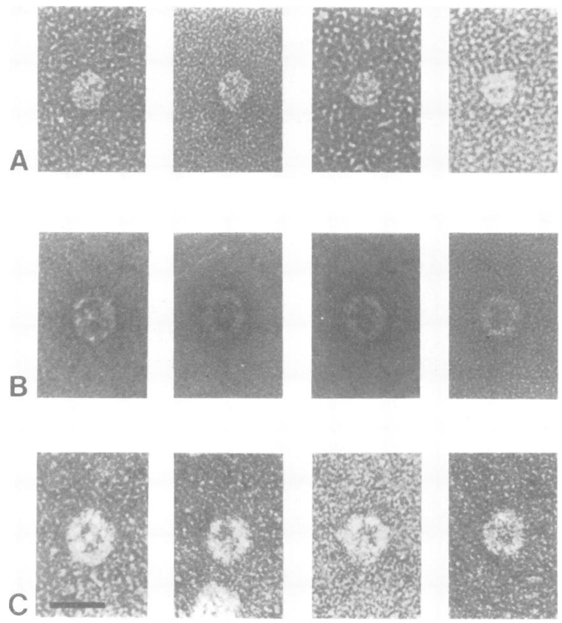

Fig. 5. A gallery of spliceosomes demonstrating the effect of the KCl concentration on the size of the spliceosome complex. Rows **A** and **B** are particles seen in spliceosome preparations that were first run on a gradient containing 400 mM KCl and then layered onto a 25-mM or 100-mM KCl gradient respectively. In row A the average size of the particle was 16 × 18 ± 1.5 nm. In row B the average size of the particle was 20 × 23.5 ± 1.5 nm. Row **C** shows particles seen in a spliceosome preparation that had been run only on the 400-mM KCl gradient; here the average particle size was 23 × 25 ± 1.5 nm. Bar = 25 nm.

(Figure 5, row B) they were 20 nm × 23.5 ± 1.5 nm, and at 400 mM KCl (Figure 5, row C) they were 23 nm × 25 ± 1.5 nm. The salt-dependent change in spliceosome size as a consequence of salt concentration can explain the observed differences in sedimentation rates. The increase in the spliceosome size would lead to a higher frictional coefficient while the particle constituents remained the same. The change in dimensions observed for this ovoid particle is consistent with the change of sedimentation rate for the spliceosome brought about by different salt concentrations and supports the conclusion that this particle is the spliceosome. Furthermore, the heterogeneity in the shape of the spliceosome could also be discerned in the 25-mM and 400-mM KCl fractions, as well as the 100-mM KCl fractions (compare Figure 5 leftmost ovoids to the rightmost circles). This heterogeneity in spliceosome size and shape appears to be an intrinsic spliceosome characteristic.

Discussion

The observed particle is the spliceosome by six criteria: (i) it forms only in the presence of ATP and active pre-mRNA; (ii) the concentration of the particles in the electron microscope correlates with radioactivity in the 40S peak gradient fractions; (iii) oligostreptavidin rods will attach to biotinylated pre-mRNA contained within these spliceosomes; (iv) T4 gp32 attaches to the pre-mRNA incorporated in the spliceosome; (v) antibodies directed against spliceosome proteins attach to the complexes; and (vi) the salt-dependent changes in size of the particle can explain the change in sedimentation rate that is observed. The yeast spliceosome dimensions in 100 mM KCl are approximately the same dimensions, 20 nm × 23 nm, as the mammalian hnRNP disc, 20−22 nm (Karn *et al.*, 1977; LeStourgeon *et al.*, 1977; Wooley *et al.*, 1986). The mammalian hnRNP has been reported also to sediment on a glycerol gradient at ~40S (LeStourgeon *et al.*, 1977). So the dimensions of the ovoid particle shown here for the yeast spliceosome are within the expected range for a disc-shaped, 40S sedimenting particle. Beyer and co-workers (Beyer and Miller, 1980; Beyer *et al.*, 1981) have seen particles 30−40 nm in diameter on preparations of *Drosophila* chorion transcripts, which they think are involved in mRNA splicing and are presumably spliceosomes. The yeast spliceosome dimensions we report here are smaller than that reported for the *Drosophila* particle, but the experimental procedures used to reveal these two particles are sufficiently different that the dimension observed for each particle cannot readily be compared. The mammalian spliceosome sediments at ~50−60S (Frendewey and Keller, 1985); its dimension should thus be slightly larger than the yeast spliceosome.

Reed and co-workers (1988) have recently reported a purification and electron microscopic identification of the mammalian spliceosome. By the electron microscopic sample preparation, they used rotary metal-shadowing, they observed a particle 40−60 nm in diameter. As expected, the mammalian spliceosome is larger in dimensions than the yeast spliceosome. The mammalian spliceosome isolated by Reed *et al.* (1988) varied in morphology from an irregular, elongated structure to a more globular ellipsoid. From the published micrographs (Reed *et al.*, 1988), the globular ellipsoid appeared to be the predominant species. In comparing the globular ellipsoid of the mammalian spliceosome with the image seen for the yeast spliceosome, an ovoid disc, the different methods of electron microscopic sample preparation must be taken into account: rotary metal-shadowing versus single-layer carbon/uranyl acetate negative staining. A similar situation of varied appearance of the same structure as the result of these two electron microscopic sample preparation methods occurred for the *Escherichia coli* 30S ribosomal subunit. By rotary metal-shadowing the 30S ribosome had a more bulbous, three-dimensional appearance showing many surface contours (Vasiliev, 1974) while a smooth, flattened, more two-dimensional image of the 30S ribosome was obtained by the single-layer carbon/uranyl acetate negative staining technique (Lake, 1979). With these considerations on sample preparation and the larger size of the mammalian spliceosome, we think that the globular ellipsoid image seen for the mammalian spliceosome and the ovoid disc seen for the yeast spliceosome are the products of variations caused by the electron microscopic sample preparation techniques. The overall morphologies of the mammalian and yeast spliceosomes should be similar, while details in the structure will most likely vary.

As reported in this paper, there is a heterogeneity in diameter and shape of the yeast spliceosomes seen in a single 40S peak fraction. These variations in the particle morphology could possibly indicate that the spliceosomes were damaged or denatured by the isolation procedure. Although the possibilty of partially denatured spliceosomes cannot be completely eliminated, still each of the different diameter particles reported could be found with the various spliceosome marker molecules attached. We think the heterogeneity seen for these particles may be the visual representation of the dynamic process that is pre-mRNA splicing (Konarska and Sharp, 1986; Pikielny *et al.*, 1986; Cheng and Abelson, 1987). A variety of experiments can be done to correlate the different observed morphologies of the spliceosome with the known intermediate stages of the splicing process. By using pre-mRNAs with mutated splicing signals (Vijayraghaven *et al.*, 1986), specific buffer conditions (Cheng and Abelson, 1987) or the existing *rna* mutants (Lustig *et al.*, 1986), the spliceosome might be 'frozen' into a particular intermediate conformation. Identification of the specific structural aspects of these particular spliceosome intermediates will provide information that will allow us to assign the various spliceosome conformations to the stages of the splicing process.

With the identification of common structures for the spliceosome, experiments can be done to identify the positions of the individual splicing components on this particle. Antibodies to other yeast spliceosome protein components, the RNA gene products, are now being produced. These proteins (e.g. *RNA*11 used in this paper) have been shown to be intimately involved in mRNA splicing (Lustig *et al.*, 1986; Chang *et al.*, 1988). These new antibodies can be used for immune EM labeling of the spliceosome to determine where the various proteins are located on the complex. Also, biotin labeled RNAs complementary to regions of the pre-mRNA or to the snRNA components of the snRNP can be used to map the location of RNAs in the spliceosome. Similar RNA mapping experiments have been successfully done for regions of the 16S rRNA on the *E.coli* 30S ribosome (Oakes *et al.*, 1986). Such three-dimensional information for the spliceosome will be invaluable for understanding the macromolecular mechanism of mRNA splicing.

Materials and methods

mRNA splicing assays

mRNA splicing extracts were prepared from yeast strain 20-1-20, obtained from E.Jones, using the procedure of Lin *et al.* (1985). Preparation of the precursor mRNA, a yeast actin transcript with truncated exon 1 and exon 2, was prepared as described in Cheng and Abelson (1986). The mRNA splicing assay was carried out as reported in Lin *et al.* (1985).

Double glycerol gradient purification of the spliceosome

0.2 ml of pre-mRNA splicing extract was layered on an 11 ml, 7−19% linear glycerol gradient containing 20 mM Na-phosphate, pH 7.5, 2 mM $MgCl_2$, 400 mM KCl, 1 mM DTT. This gradient was centrifuged in a SW41 rotor (Beckman) for 4 h at 40 000 r.p.m. at 6°C. The gradient was then fractionated, and the radioactivity profile was determined from Cerenkov emission for each fraction. The spliceosome peak fractions were pooled and loaded on a 5 ml, 15−27% linear glycerol gradient containing 20 mM Na-phosphate, pH 7.5, 2 mM $MgCl_2$, 100 ml KCl, 1 mM DTT. This gradient was centrifuged in a SW55 rotor (Beckman) for 1.5 h at 50 000 r.p.m. at 6°C, and then fractionated.

Labeling of the spliceosome for electron microscopy

Each of the electron microscopic tags used for the spliceosome labeling was added to spliceosome fractions taken from a glycerol gradient containing 400 mM KCl. The specific tag was added in the appropriate concentration (see Figure 4 legend for details) and then incubated at 10°C for 15 min. The tagged sample was then layered onto a gradient containing 100 mM KCl and centrifuged as stated above. Oligomerized streptavidin (OSA) rods were prepared by polymerizing streptavidin (BRL) with a bifunctional biotin reagent as detailed in Green *et al.* (1971). The OSA rods were then fractionated on a G100 Sephadex (Pharmacia) column and rod size was determined by EM. The T4 gene 32 protein product was purchased from Pharmacia. The IgG fraction of the anti-Sm58 and anti-RNA11 antiserum was purified on a Protein A−Sepharose (Sigma) column by standard procedures (Chang *et al.*, 1988).

Electron microscopy staining

Immediately after fractionation of the final 5-ml gradient, 70% glutaraldehyde (Polyscience) was added to the entire fraction to make a final concentration of 0.3% (Valentine *et al.*, 1968). These samples were incubated on ice for 10–20 min. The radioactivity of the fixed fractions was determined from Cerenkov emission, and then the fractions were stained for EM by the single-layer carbon staining method of Lake (1979). For this staining procedure a carbon film was vacuum evaporated onto the surface of a freshly cleaved sheet of mica. A small piece of this mica/carbon film was cut and placed into the sample solution in such a way that the carbon film pulled away from the mica and floated on the surface of the sample. The carbon film remained exposed to the sample for 20–30 s to allow the spliceosomes to adhere to the charged carbon surface. In these experiments the carbon film was first treated with 2.5 μg/ml of bacitracin (Sigma) to increase its binding capacity before being placed into the fixed sample (Gregory and Pirie, 1973). The carbon film with sample attached was then floated onto a 1% aqueous uranyl acetate solution, allowed to remain there for 30 s, then it was picked up on a hexagonal bar, 400 mesh EM grid (SPI). Excess stain was removed from the grid by placing it face up and flatly onto a piece of 3MM Whatman filter paper. The grid was allowed to air dry before storage. The grids were viewed on a Phillips 201B EM.

Acknowledgements

We thank Drs T.H.Chang, S.-C.Cheng, G.McFarland, E.Phizicky, K.Tanner and S.Westaway for critical comments on the manuscript and helpful discussion. We especially thank Drs S.Hoch and T.H.Chang for providing anti-Sm58 and anti-RNA11 respectively. This work was supported by National Institutes of Health Postdoctoral fellowship No. 5732 GM 1008-02 to M.W.C. and National Institutes of Health grant GM 32637 to J.N.A.

References

Beyer,A.L. and Miller,O.L. (1980) *Cell*, **20**, 75–84.
Beyer,A.L. and Osheim,Y.J. (1988) *Genes Dev.*, **2**, 754–765.
Beyer,A.L., Bouton,A.H. and Miller,O.L. (1981) *Cell*, **26**, 155–165.
Bindereif,A. and Green,M.R. (1987) *EMBO J.*, **6**, 2415–2424.
Black,D.L. and Steitz,J.A. (1986) *Cell*, **46**, 697–704.
Black,D.L., Chabot,B.C. and Steitz,J.A. (1985) *Cell*, **42**, 737–750.
Brody,E. and Abelson,J.A. (1985) *Science*, **228**, 963–967.
Chabot,T. and Steitz,J.A. (1987) *Mol. Cell. Biol*, **7**, 281–293.
Chang,T.H., Clark,M.W., Cusick,M. and Abelson,J. (1988) *Mol. Cell. Biol.*, **8**, 2379–2393.
Cheng,S.C. and Abelson,J. (1986) *Proc. Natl. Acad. Sci. USA*, **81**, 1991–1995.
Cheng,S.C. and Abelson,J. (1987) *Genes Dev.*, **1**, 1014–1027.
Frendewey,D. and Keller,W. (1985) *Cell*, **42**, 355–361.
Grabowski,P.J. and Sharp,P.A. (1986) *Science*, **233**, 1294–1299.
Grabowski,P.J., Seiler,S.R. and Sharp,P.A. (1985) *Cell*, **42**, 345–353.
Green,N.M., Konieczny,L., Toms,E.J. and Valentine,R.C. (1971) *Biochem. J.*, **125**, 781–791.
Gregory,D.W. and Pirie,B.J.S. (1973) *J. Microscopy*, **99**, 261–265.
Hartwell,H.L. (1967) *J. Bacteriol.*, **93**, 1662–1670.
Karn,J., Vidali,G., Boffa,L.C. and Allfrey,V.G. (1977) *J. Biol. Chem.*, **252**, 7307–7322.
Konarska,M. and Sharp,P.A. (1986) *Cell*, **46**, 845–855.
Lake,J.A. (1979) *Methods Enzymol.*, **61**, 250–257.
Lake,J.A., Henderson,E., Oakes,M. and Clark,M.W. (1984) *Proc. Natl. Acad. Sci. USA*, **81**, 3786–3790.
LeStourgeon,W.M., Beyer,A.L., Christensen,M.E., Walker,B.W., Poupore,S.M. and Daniels,L.P. (1977) *Cold Spring Harbor Symp. Quant. Biol.*, **42**, 885–898.
Lin,R.-J., Lustig,A.J. and Abelson,J. (1987) *Genes Dev.*, **1**, 7–18.
Lin,R.-J., Newman,A.J., Cheng,S.C. and Abelson,J. (1985) *J. Biol. Chem.*, **260**, 14780–14792.
Lossky,M., Anderson,G.J., Jackson,S.P. and Beggs,J. (1987) *Cell*, **51**, 1019–1026.
Lustig,A.J., Lin,R.-J. and Abelson,J. (1986) *Cell*, **47**, 953–963.
Mount,S.M. and Steitz,J.A. (1984) *Mol. Cell. Biol.*, **3**, 249–297.
Maniatis,T. and Reed,R. (1987) *Nature*, **325**, 673–678.
Newport,J.W., Lonberg,N., Kowalczykowowsi,S.C. and Von Hippel,P.H. (1981) *J. Mol. Biol.*, **169**, 105–121.
Oakes,M.I., Clark,M.W., Henderson,E. and Lake,J.A. (1986) *Proc. Natl. Acad. Sci. USA*, **83**, 275–279.
Osheim,Y.N., Miller,O.L. and Beyer,A.L. (1985) *Cell*, **43**, 143–151.
Pikielny,C.W., Rymond,B.C. and Rosbash,M. (1986) *Nature*, **324**, 341–345.
Reed,R., Griffith,J. and Maniatis,J. (1988) *Cell*, **53**, 949–961.
Riedel,N., Wolin,S. and Guthrie,C. (1987) *Science*, **235**, 328–331.
Rosbash,M., Wittanris,P.K., Woolford,J.L. and Teem,J.L. (1981) *Cell*, **24**, 679–686.
Sharp,P.A. (1987) *Science*, **235**, 766–771.
Soltyk,A., Tropak,M. and Friesen,J.D. (1984) *J. Bacteriol.*, **160**, 1093–1100.
Stoops,J.K., Awad,E.S., Arsianian,M.J., Gunsberg,S, and Wakil,S.J. (1978) *J. Biol. Chem.*, **253**, 4464–4475.
Thomas,J.O., Glowacka,S.K. and Szer,W. (1983) *J. Mol. Biol.*, **171**, 439–455.
Tollervey,D. and Mattaj,I.W. (1987) *EMBO J.*, **6**, 469–476.
Valentine,R.C., Shapiro,B.M. and Stadtman,E.R. (1968) *Biochemistry*, **7**, 2143–2152.
Vasiliev,V.D. (1974) *Acta Biol. Med. Ger.*, **33**, 779–793.
Vijayraghaven,U., Parker,R., Tamm,J., Iimura,Y., Rossi,J., Abelson,J. and Guthrie,C. (1986) *EMBO J.*, **5**, 1683–1695.
Wooley,J., Chung,S.-Y., Wall,J. and LeStourgeon,W. (1986) *Biophys. J.*, **49**, 17–19.

Received on July 14, 1988; revised on August 25, 1988